MAINLOBE AND PEAK SIDELOBE CONTROL IN ADAPTIVE ARRAYS

Renbiao Wu[†] *Zhisong Wang*[‡] *Jian Li*[‡] *

[†] Institute of Communications and Information Processing, P.O.Box 9
Civil Aviation University of China, Tianjin, 300300, P.R.China.

[‡] Department of Electrical and Computer Engineering, University of Florida, P.O. Box 116130, Gainesville, FL 32611, USA.

ABSTRACT

In radar applications, adaptive beampatterns with low sidelobes and stable mainlobe shapes are desired to suppress pulsed deceptive jammers or sidelobe targets and to accurately measure the direction-of-arrival (DOA) of a target using monopulse techniques. In practice, all kinds of errors exist, such as signal pointing errors, array calibration errors and array covariance matrix estimation errors. In the presence of these errors, adaptive beamformers can suffer from severe performance degradations, including poor interference rejection, distorted mainlobes, and high sidelobes. In this paper, we investigate how a quadratic constraint based adaptive beamformer with peak sidelobe control, referred to as the PPSC (Precise Peak Sidelobe Control) method, can be combined with a signal removal scheme to achieve desired adaptive beampatterns and interference rejection performance for a uniform linear array. Numerical results are provided to demonstrate the performance of the proposed method.

1. INTRODUCTION

Modern radars use a variety of electronic counter-counter-measures (ECCM) to suppress both intentional jamming (including long-duty-cycle jammers and pulsed deceptive jammers) and inadvertent interference (clutter, densed sidelobe targets, etc.) [1]. Adaptive beamformers designed for radar antenna arrays (also called adaptive arrays) have proven to be a very effective ECCM technique [2]. Adaptive beamforming is very effective for long-duty-cycle interference (continuous jammers and clutter) rejection since their statistics can be estimated from multiple available data samples with identical or similar statistical distributions. However, target-like pulsed deceptive jammers and sidelobe targets are difficult to suppress since their duration time is too short. They can only be mitigated by low sidelobes. Tracking requires accurate measurement of the target position. Monopulse techniques [3] are usually used to determine the DOA of a target within a fraction of a beamwidth by comparing the measurements received in two or more simultaneous beams (such as the sum and difference beams). Stable mainlobe shapes are critically needed for the accurate estimation of the DOA of a target via the monopulse techniques. Hence, adaptive beamformers in radar applications often need to have adaptive beampatterns with low peak sidelobes, stable mainlobes, and deep nulls in the incident angles of long-duty-cycle interference.

Almost all of the adaptive beamforming approaches, such as, for example, the standard Capon beamformer (SCB) [4] and the robust Capon beamformer (RCB) [5] are mainly concerned with interference rejection while peak sidelobe control is not considered.

In [6], a quadratic constraint based algorithm, referred to as the Precise Peak Sidelobe Control (PPSC) approach was proposed. PPSC is a diagonal loading approach but the diagonal loading level can be determined according to the Desired Peak Sidelobe Level (DPSL) for uniform linear arrays. In this paper, the effects of the presence of target signals on PPSC are investigated and we show how PPSC can be combined with a signal removal scheme for improved mainlobe control performance.

2. PRECISE PEAK SIDELOBE CONTROL (PPSC)

Consider a uniform linear array comprised of N elements. The received data vector can be modeled as

$$\mathbf{x}(m) = s(m)\mathbf{a}(\theta_s) + \mathbf{x}_I(m) + \mathbf{e}(m),\ m = 1, 2, \cdots, M \quad (1)$$

where $\mathbf{x}(m)$ is the mth snapshot, M is the number of snapshots, $s(m)$ denotes the target signal, $\mathbf{x}_I(m)$ is the interference data vector, $\mathbf{e}(m)$ denotes the receiver noise vector which is modeled as a zero-mean spatially white Gaussian random process, and $\mathbf{a}(\theta_s)$ denotes the array steering vector of the target:

$$\mathbf{a}(\theta_s) = \left[\ \exp(j\tfrac{2\pi d}{\lambda}\sin\theta_s) \quad \cdots \quad \exp(j\tfrac{2\pi Nd}{\lambda}\sin\theta_s)\ \right]^T \quad (2)$$

with $(\cdot)^T$ denoting the transpose, d being the element spacing, λ the wavelength, and θ_s the direction of arrival (DOA) of the target.

The sample covariance matrix is defined as

$$\hat{\mathbf{R}} = \frac{1}{M}\sum_{m=1}^{M}\mathbf{x}(m)\mathbf{x}^H(m) \quad (3)$$

where $(\cdot)^H$ denotes the conjugate transpose.

Let $\mathbf{a}_q$ denote the quiescent weight vector, which is usually designed to produce beampatterns (called quiescent beampatterns) with desired mainlobe beamwidth and low peak sidelobes. In this paper, we design $\mathbf{a}_q$ as follows:

$$\mathbf{a}_q = \left[\ I_1\exp(j\tfrac{2\pi d}{\lambda}\sin\theta_0) \quad \cdots \quad I_N\exp(j\tfrac{2\pi Nd}{\lambda}\sin\theta_0)\ \right]^T \quad (4)$$

where $\{I_n\}_{n=1}^N$ are the tapper settings (e.g., Chebyshev or Taylor weights) and θ_0 denotes the pointing angle. Without loss of generality, we assume that the tapper settings satisfy $\sum_{n=1}^N I_n = 1$.

In [6], a quadratic constraint based approach, referred to as the Precise Peak Sidelobe Control (PPSC), was proposed, which finds the adaptive weight vector as follows:

$$\min_{\mathbf{w}}\ \mathbf{w}^H\hat{\mathbf{R}}\mathbf{w} \quad (5)$$

$$\text{subject to} \qquad \|\mathbf{w} - \mathbf{a}_q\| \le \varepsilon_1 \quad (6)$$

*This work was supported in part by the National Science Foundation Grants ECS-0097636 and CCR-0104887 and by the National Natural Science Foundation of China under Grant 60272049 and 69902009 and the Excellent Young Teachers Program of MOE, P.R.China.

where ε_1 is a small positive value satisfying $\varepsilon_1 < \|\mathbf{a}_q\|$ (to guarantee a nonzero or nontrivial solution). The constraint defined in (6) is used to control the difference between the adaptive and desired quiescent beampatterns. We can explicitly relate ε_1 to the Desired Peak Sidelobe Level (DPSL) by using the following expression

$$\text{DPSL (dB)} = 11 + 10\log_{10}\frac{\varepsilon_1^2}{2} \tag{7}$$

By choosing ε_1 using (6), the peak sidelobe level is achieved with a probability of 99.9%.

To solve (5) and (6), we first compute the eigendecomposition of $\hat{\mathbf{R}}$

$$\hat{\mathbf{R}} = \mathbf{U}\Lambda\mathbf{U}^H \tag{8}$$

where

$$\mathbf{U} = \left[\begin{array}{cccc} \mathbf{u}_1 & \mathbf{u}_2 & \cdots & \mathbf{u}_N \end{array}\right] \tag{9}$$

and

$$\Lambda = \text{diag}\left[\begin{array}{cccc} \lambda_1, & \lambda_2, & \cdots, & \lambda_N \end{array}\right] \tag{10}$$

with $\mathbf{u}_n$ and λ_n ($\lambda_1 \geq \lambda_2 \geq \cdots \geq \lambda_N$) denoting the nth eigenvector and the nth eigenvalue of $\hat{\mathbf{R}}$, respectively. By using the Lagrange multiplier technique, we get

$$\mathbf{w}_{\text{PPSC}} = \eta(\hat{\mathbf{R}} + \eta\mathbf{I})^{-1}\mathbf{a}_q \tag{11}$$

Note that PPSC is a diagonal loading approach and the diagonal loading value ($\eta > 0$) is precisely determined by solving the following equation

$$f(\eta) \triangleq \sum_{n=1}^{N}\left(\frac{\lambda_n}{\eta+\lambda_n}\right)^2 |a_q(n)|^2 = \varepsilon_1^2 \tag{12}$$

where $a_q(n)$ denotes the nth element of the vector $\mathbf{a}_q$.

Note also that $f(\eta)$ is a monotonically decreasing function of $\eta > 0$. Since $f(0) = \|\mathbf{a}_q\|^2 > \varepsilon_1^2$ and $f(\infty) = 0 < \varepsilon_1^2$, the solution of η is unique. Note that [6]

$$\frac{\lambda_N(\|\mathbf{a}_q\| - \varepsilon_1)}{\varepsilon_1} \leq \eta \leq \frac{\lambda_1(\|\mathbf{a}_q\| - \varepsilon_1)}{\varepsilon_1} \tag{13}$$

The solution η to (12) can be efficiently determined by using, e.g., the Newton's method, within the interval in (13). Hence PPSC requires $O(N^3)$ flops.

3. EFFECTS OF THE PRESENCE OF TARGET SIGNALS AND THEIR REMOVAL

By using $\hat{\mathbf{R}}^{-1} = \sum_{n=1}^{N}\frac{1}{\lambda_n}\mathbf{u}_n\mathbf{u}_n^H$, the adaptive beampattern obtained by PPSC ($G_{\text{PPSC}}(\theta)$) can be decomposed as follows

$$\begin{aligned} G_{\text{PPSC}}(\theta) &= \mathbf{w}_{\text{PPSC}}^H\mathbf{a}(\theta) && (14)\\ &= G_q(\theta) - \sum_{n=1}^{N}\frac{\lambda_n-\lambda_N}{\lambda_n+\eta}\beta_n G_n(\theta) && (15)\end{aligned}$$

where $G_q(\theta) = \mathbf{a}_q^H\mathbf{a}(\theta)$ denotes the quiescent beampattern, $G_n(\theta) = \mathbf{u}_n^H\mathbf{a}(\theta)$ denotes the nth eigen beampattern, and $\beta_n = \mathbf{a}_q^H\mathbf{u}_n$ represents the spatial correlation between the steering vector and the nth eigenvector.

Define the perturbation beampattern after adaptive processing with PPSC as

$$\begin{aligned} \Delta G(\theta) &= G_{\text{PPSC}}(\theta) - G_q(\theta) && (16)\\ &= -\sum_{n=1}^{N}\frac{\lambda_n-\lambda_N}{\lambda_n+\eta}\beta_n G_n(\theta) && (17)\end{aligned}$$

Then the average power Q of the perturbation beampattern satisfies

$$\begin{aligned} Q &\triangleq \frac{1}{\pi}\int_{-\frac{\pi}{2}}^{\frac{\pi}{2}} |\Delta G(\theta)|^2\, d\theta && (18)\\ &= \frac{1}{\pi}\int_{-\frac{\pi}{2}}^{\frac{\pi}{2}} |(\mathbf{w}-\mathbf{a}_q)^H\mathbf{a}(\theta)|^2\, d\theta && (19)\\ &\leq \frac{1}{\pi}\int_{-\frac{\pi}{2}}^{\frac{\pi}{2}} \|(\mathbf{w}-\mathbf{a}_q)\|^2\|\mathbf{a}(\theta)\|^2\, d\theta && (20)\\ &= N\|\mathbf{w}-\mathbf{a}_q\|^2 && (21)\\ &\leq N\varepsilon_1^2 && (22)\end{aligned}$$

For simplicity, assume that the received data consist of only one target signal and the receiver noise and

$$\hat{\mathbf{R}} = \mathbf{R} = \sigma_s^2\mathbf{a}(\theta_s)\mathbf{a}^H(\theta_s) + \sigma_e^2\mathbf{I} \tag{23}$$

where σ_s^2 and σ_e^2 denote the powers of the target signal and noise, respectively. In this case, the perturbation beampattern can be written as

$$\Delta G(\theta) = -\frac{N\sigma_s^2}{N\sigma_s^2+\sigma_e^2+\eta}\beta_1 G_1(\theta) \tag{24}$$

where

$$\beta_1 = \frac{1}{\sqrt{N}}\mathbf{a}_q^H\mathbf{a}(\theta_s) = \frac{1}{\sqrt{N}}\sum_{n=1}^{N} I_n e^{j\frac{2\pi n d}{\lambda}(\sin\theta_s - \sin\theta_0)} \tag{25}$$

and

$$G_1(\theta) = \frac{1}{\sqrt{N}}\mathbf{a}^H(\theta_s)\mathbf{a}(\theta) = \frac{1}{\sqrt{N}}\sum_{n=1}^{N} e^{-j\frac{2\pi n d}{\lambda}(\sin\theta_s - \sin\theta)} \tag{26}$$

Note that since Q is bounded by (22), the smaller the signal pointing error ($|\theta_s - \theta_0|$), the larger the diagonal loading value. Also, the higher the σ_s^2, the larger the diagonal loading value.

To reduce the high sidelobes due to the spread of small noise eigenvalues caused by the covariance matrix estimation errors, a small diagonal loading value is enough. However, it can be noted from (24) that when the SNR is high or the pointing error is small, a much larger diagonal loading value is needed for mainlobe shape control, which may cause performance loss for weak interference rejection. Below we give a signal removal procedure to deal with this problem.

Define

$$s = \arg\max_n \{|\beta_n|, n = 1, 2, \cdots, N\} \tag{27}$$

where β_n is the spatial correlation between $\mathbf{a}_q$ and the $\mathbf{u}_n$ as defined in (15). Then $\mathbf{u}_s$ is the closest eigenvector to the steering vector $\mathbf{a}_q$. If $|\beta_s|$ exceeds a predetermined threshold, say γ, then we can assume there is a target and determine the covariance matrix after signal removal by

$$\hat{\mathbf{R}}_{\text{I+N}} = \hat{\mathbf{R}} - \lambda_s\mathbf{u}_s\mathbf{u}_s^H \tag{28}$$

By replacing $\hat{\mathbf{R}}$ in (5) with $\hat{\mathbf{R}}_{\text{I+N}}$ in (28) we can obtain a new algorithm, referred to as the Signal Removal PPSC (SR-PPSC) method. Because of the covariance matrix estimation errors, the signal removal is incomplete. However, since PPSC itself is very robust against pointing and covariance matrix estimation errors, incomplete signal removal is not a big problem and PPSC can deal with it effectively. In addition, SR-PPSC also requires $O(N^3)$ flops.

4. EFFECTS OF ARRAY ERRORS AND REMEDIES

In practice, there also exist array calibration errors. Denote the array manifold vector with calibration errors as

$$\tilde{\mathbf{a}}(\theta) = (\mathbf{I} + \mathbf{P})\mathbf{a}(\theta) \tag{29}$$

where

$$\mathbf{P} = \text{diag}\{\delta_1 + j\phi_1, \delta_2 + j\phi_2, \cdots, \delta_N + j\phi_N\} \tag{30}$$

with δ_n and ϕ_n denoting the random amplitude and phase errors, respectively. Assume δ_n and ϕ_n are independent zero-mean Gaussian random variables with variance σ_δ^2 and σ_ϕ^2, respectively. Then the peak sidelobe level of the true quiescent beampatterns in the presence of calibration errors can be determined by [6, 7]

$$\text{PSL (dB)} \quad = \quad 11 + 10\log_{10}\frac{\|\mathbf{a}_q\|^2(\sigma_\delta^2 + \sigma_\phi^2)}{2} \tag{31}$$

where $\sum_{n=1}^{N} I_n = 1$ is used. Note from (31) that for large calibration errors, the peak sidelobe level is mainly determined by the calibration error variance, no matter how low the peak sidelobe level of the designed quiescent beampatterns is. Roughly speaking, the achievable peak sidelobe level is nearly independent of the weight settings in the presence of array calibration errors.

In the presence of array calibration errors, PPSC and SR-PPSC can still work but the soft constraint factor ε_1^2 must be determined by

$$\text{DPSL (dB)} = 11 + 10\log_{10}\frac{\|\mathbf{a}_q\|^2(\varepsilon_1^2 + \sigma_\delta^2 + \sigma_\phi^2)}{2} \tag{32}$$

5. NUMERICAL RESULTS

In this section, we present several numerical examples to evaluate the performance of the proposed SR-PPSC algorithm. Assume that the uniform linear array consists of $N = 32$ elements with element spacing $d = 0.5\lambda$. Assume that one target and two jammers impinge on the array with incident angles $\theta_s = 2.0^\circ$, $\theta_1 = 30^\circ$, and $\theta_2 = -30^\circ$, respectively. The received data vector can be written as

$$\mathbf{x}(m) = s(m)\tilde{\mathbf{a}}(\theta_s) + J_1(m)\tilde{\mathbf{a}}(\theta_1) + J_2(m)\tilde{\mathbf{a}}(\theta_2) + \mathbf{e}(m) \tag{33}$$

$$= s(m)\tilde{\mathbf{a}}(\theta_s) + \mathbf{x}_I(m) + \mathbf{e}(m), m = 1, 2, \cdots, M \tag{34}$$

The powers for the target signal $s(m)$ and the jammers $J_i(m)$, $i = 1, 2$, are denoted by $\sigma_s^2 = E\left[|s(m)|^2\right]$ and $\sigma_i^2 = E\left[|J_i(m)|^2\right]$, $i = 1, 2$, respectively, where $E[\cdot]$ denotes the expectation. The noise vector $\mathbf{e}(m)$ is a zero-mean white Gaussian random process with variance σ_e^2. The single channel SNR (signal-to-noise ratio) and JNR (jammer-to-noise ratio) are defined, respectively, as

$$\text{SNR} = \frac{\sigma_s^2}{\sigma_e^2} \tag{35}$$

and

$$\text{JNR}_i = \frac{\sigma_i^2}{\sigma_e^2}, \ i = 1, 2 \tag{36}$$

The output SINR (signal-to-interference-plus-noise ratio) is defined as

$$\text{SINR} = \frac{\sigma_s^2|\hat{\mathbf{w}}^H\tilde{\mathbf{a}}(\theta_s)|^2}{\hat{\mathbf{w}}^H\mathbf{R}_{\text{I+N}}\hat{\mathbf{w}}} \tag{37}$$

where $\hat{\mathbf{w}}$ denotes the adaptive weight vector obtained using M snapshots and

$$\mathbf{R}_{\text{I+N}} = E\left\{[\mathbf{x}_{\text{I}}(m) + \mathbf{e}(m)][\mathbf{x}_{\text{I}}(m) + \mathbf{e}(m)]^H\right\} \tag{38}$$

Unless otherwisely stated, in the following examples, we have $M = 64$, the quiescent beampattern takes the -40 dB Chebyshev weights, the pointing angle is $\theta_0 = 0^\circ$, $\text{JNR}_1 = \text{JNR}_2 = 45$ dB, and 100 Monte-Carlo trials are used to obtain beampatterns and SINR curves. The samples for both calibration errors and noise vary from trial to trial.

First, we use an example to illustrate the effects of target signals and assume that there are no array calibration errors. We set DPSL $= -25$ dB and SNR = 0 dB. Figure 1 compares the diagonal loading values used by PPSC ("$*$") and SR-PPSC ("$\circ$") as a function of the pointing error $|\theta_s - \theta_0|$. Note from Figure 1 that for the PPSC method, the larger the pointing error, the smaller the diagonal loading value. When the target enters into the sidelobe region, it will be treated as an interference and a small diagonal loading value can make the sidelobes to be below DPSL. The ratio r between the first and the second largest magnitudes of β_n, which represents the correlation between the steering vector and the nth eigenvector of $\hat{\mathbf{R}}$, is shown in Figure 2 as a function of $|\theta_s - \theta_0|$. Note that when θ_s is within the mainlobe, r $\gg 1$, which can be used to indicate the presence of a target signal. When $|\theta_s - \theta_0|$ is large (the target signal becomes interference), r $\simeq 1$.

Now we consider the effects of array calibration errors. Assume the array has a 10% calibration error (i.e., $\sigma_\delta = \sigma_\phi = 10\%$, and $\sigma_\phi = 10\%$ means $\sigma_\phi = 0.1$ radians). The ideal quiescent beampattern is shown in Figure 3(a), which is a -40 dB Chebyshev beampattern. The true beampatterns obtained using the ideal quiescent weights in the presence of calibration errors are shown in Figure 3(b). From Figures 3(a) and (b) it can be noted that, as predicted by (31), although the designed peak sidelobe level is -40 dB, the practical beampatterns have a peak sidelobe level of approximately -22 dB (i.e., PSL $= -22$ dB when the array has 10% calibration errors). In this case, we want to control the peak sidelobe level to DPSL $= -20$ dB and the adaptive beampatterns obtained via SCB, PPSC and SR-PPSC are shown in Figures 3(c), 3(d), 3(e), respectively. Note that although the quiescent beampattern has a peak sidelobe level of -40 dB, the peak sidelobes of the adaptive beampatterns obtained via SCB rise up to -2 dB. Also, SCB gives highly distorted mainlobes. On the other hand, although the margin between DPSL and PSL (limited value of the peak sidelobe level) is only 2 dB, both PPSC and SR-PPSC can precisely control the peak sidelobe level of adaptive beampatterns. The latter controls the mainlobe shape better than the former. In Figure 3, SNR = 0 dB and $\theta_s = 2^\circ$. The SINR curves of SCB, PPSC and SR-PPSC are compared in Figure 4. Note that both PPSC and SR-PPSC significantly outperform SCB and SR-PPSC performs better than PPSC for jammer suppression. This occurs because after signal removal, the diagonal loading value is significantly reduced.

6. CONCLUSIONS

Peak sidelobe control and mainlobe shape maintenance are very important for robust adaptive array processing in radar. Effects of target signals on a robust peak sidelobe control method, referred to as Precise Peak Sidelobe Control (PPSC), are investigated and a signal removal scheme is given to further improve its performance. The proposed method exhibits excellent interference rejection performance and superior beampattern control quality in the presence of various errors including signal pointing and array calibration errors.

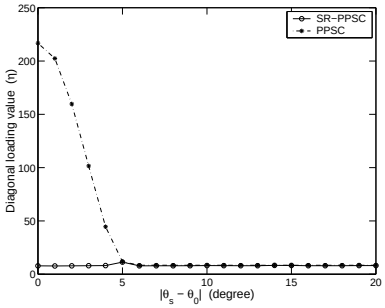

Fig. 1. Effects of signal removal on the diagonal loading value (η) when $\theta_1 = 30°$, $\theta_2 = -30°$, $\theta_0 = 0°$, $\text{JNR}_1 = \text{JNR}_2 = 45$ dB, SNR $= 0$ dB, and no array calibration errors exist.

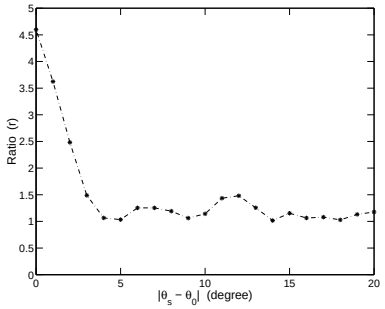

Fig. 2. Ratio (r) between the first and second largest magnitudes of the spatial correlation β_n versus $|\theta_s - \theta_0|$ when SNR = 0 dB, $\theta_1 = 30°$, $\theta_2 = -30°$, $\theta_0 = 0°$, $\text{JNR}_1 = \text{JNR}_2$= 45 dB, and no array calibration errors exist.

7. REFERENCES

[1] M. I. Skolnik, *Radar Handbook.* New York: McGraw-Hill Book Company, 1990.

[2] A. Farina, *Antenna-Based Signal Processing Techniques for Radar Systems*. Artech House, Inc., 1992.

[3] K. B. Yu and D. J. Murrow, "Adaptive digital beamforming for angle estimation in jamming," *IEEE Transactions on Aerospace and Electronic Systems*, vol. 37, pp. 508–523, April 2001.

[4] J. Capon, "High resolution frequency-wavenumber spectrum analysis," *Proceedings of the IEEE*, vol. 57, pp. 1408–1418, August 1969.

[5] P. Stoica, Z. Wang, and J. Li, "Robust Capon beamforming," *IEEE Signal Processing Letters*, 2002. To appear.

[6] R. Wu, Z. Bao, and Y. Ma, "Control of peak sidelobe level in adaptive arrays," *IEEE Transactions on Antennas and Propagation*, vol. 44, pp. 1341–1347, October 1996.

[7] J. K. Hsiao, "Normalized relationship among errors and sidelobe levels," *Radio Science*, vol. 19, pp. 292–302, Jan./Feb. 1984.

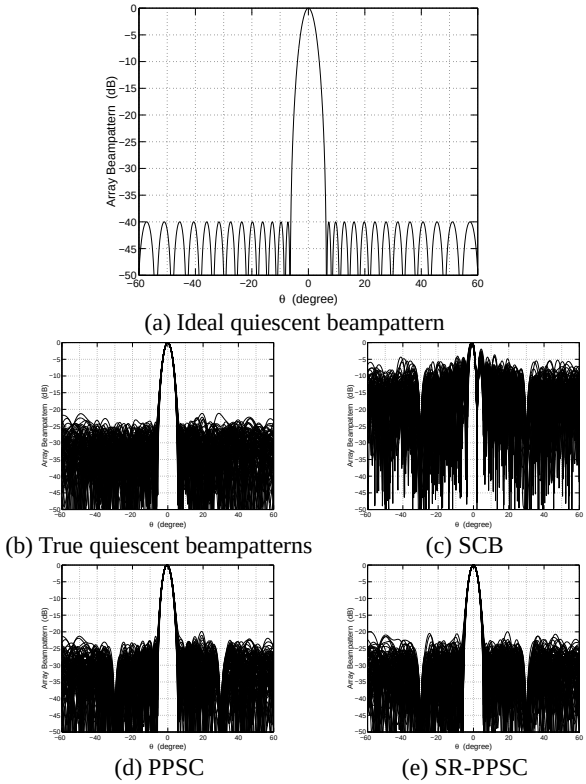

(a) Ideal quiescent beampattern

(b) True quiescent beampatterns (c) SCB

(d) PPSC (e) SR-PPSC

Fig. 3. Effects of array calibration errors on the quiescent and adaptive beampatterns. (a) Ideal quiescent beampattern without calibration errors, (b) true quiescent beampatterns with calibration errors, and adaptive beampatterns obtained via (c) SCB, (d) PPSC, and (e) SR-PPSC obtained when $\sigma_\delta = \sigma_\phi = 10\%$, $\theta_1 = 30°$, $\theta_2 = -30°$, $\theta_0 = 0°$, $\theta_s = 2.0°$, SNR $= 0$ dB, and $\text{JNR}_1 = \text{JNR}_2 = 45$ dB.

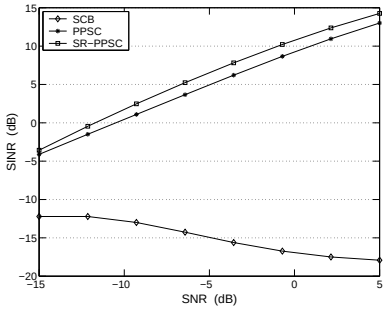

Fig. 4. Comparison of the jammer suppression performance (SINR) for SCB ("$\diamond$"), PPSC ("$*$") and SR-PPSC ("$\square$") in the presence of both pointing and array calibration errors. $\theta_1 = 30°$, $\theta_2 = -30°$, $\theta_0 = 0°$, $\theta_s = 2.0°$, $\text{JNR}_1 = \text{JNR}_2 = 45$ dB, $\sigma_\delta = \sigma_\phi = 10\%$.